RESEARCH ARTICLE SUMMARY

BIOMECHANICS

Why the seahorse tail is square

Michael M. Porter,* Dominique Adriaens, Ross L. Hatton, Marc A. Meyers, Joanna McKittrick

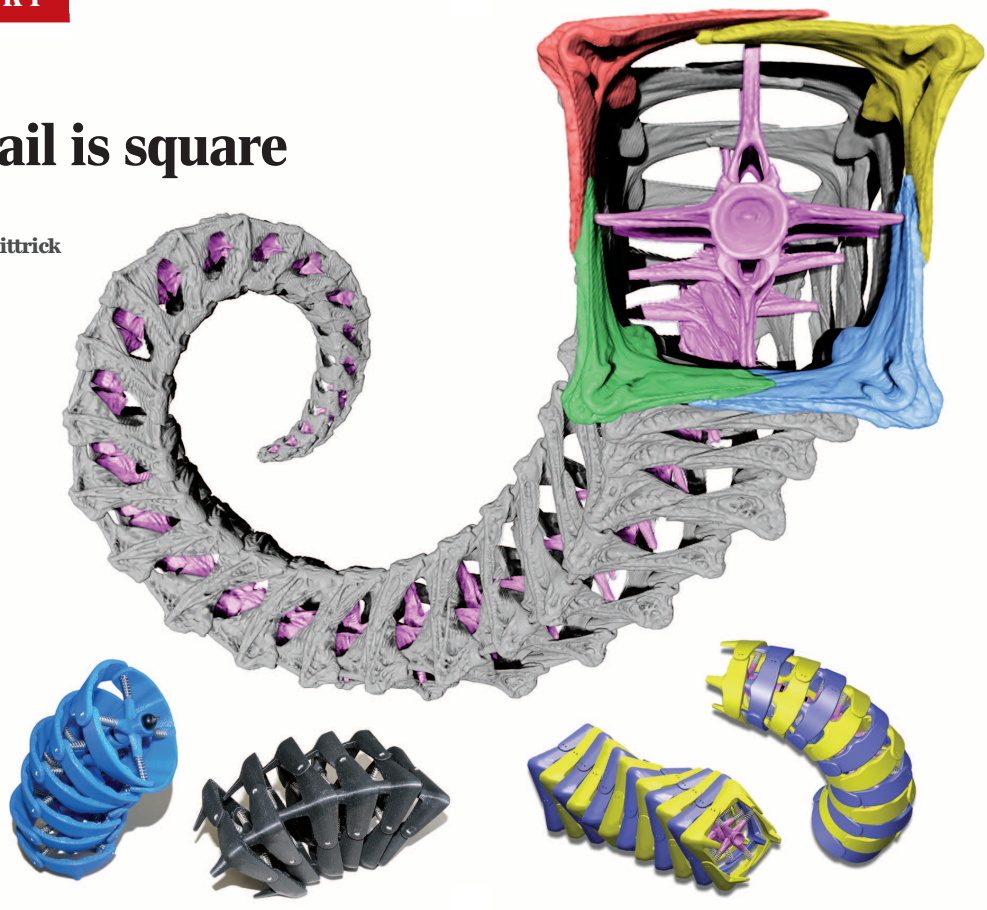

Engineering designs answer biological questions. 3D-printed models that mimic a seahorse tail were designed not only for potential engineering applications but also to answer the biological question, why might tails organized into square prisms be better than cylinders? A mechanical comparison of the prototypes shows that articulated square prisms perform better than do cylinders for grasping and resistance to crushing.

INTRODUCTION: Although the predominant shapes of most animal tails are cylindrical, seahorse tails are square prisms. The skeleton of their tails consists of a bony armor arranged into several ringlike segments composed of four L-shaped plates that surround a central vertebra. These plates articulate with specialized joints that facilitate bending and twisting, as well as resist vertebral fracture from crushing. Muscles attached to the vertebral column transmit forces to the bony plates to provide motion for grasping and holding on to objects such as sea grasses, mangrove roots, and coral reefs, which allows them to hide and rely on camouflage when evading predators and capturing prey.

RATIONALE: We hypothesize that the square cross-sectional architecture of a seahorse tail improves mechanical performance in prehension (grasping ability) and armored functions (crushing resistance), relative to a cylindrical one. To test this hypothesis, we evaluated the mechanics of two three-dimensional (3D)–printed prototypes composed of articulating plates and vertebrae that mimic the natural (square prism) and a hypothetical (cylindrical) tail structure. We compared the bending, twisting, and compressive behavior of the biomimetic prototypes to show that the square profile is better than the circular one for two integrated functions: grasping ability and crushing resistance.

RESULTS: Seahorse tails (and the prototypes) have three primary joints that enable motion: ball-and-socket, peg-and-socket, and gliding. The ball-and-socket joints connect adjacent vertebrae and constrain bending in both the square and cylindrical prototypes to the same degree, exhibiting a behavior similar to that of a natural seahorse tail. The peg-and-socket joints connect the plates of adjacent segments and substantially restrict twisting in the prototype with a square profile, as compared with the circular one. The square geometry limits excessive torsion and preserves articulatory organization, which could provide seahorses a natural safety factor against torsion-induced damage and assist in tail relaxation. Further, the square architecture is flat (increasing surface contact) and undergoes an exterior shape change when twisted, which could allow seahorses to grasp objects with more control. Gliding joints are present at the plate overlaps along all four sides of both prototypes. Under transverse compression and impact (with a rubber mallet), the plates of the square prototype slide past one another with one degree of translation freedom (analogous to the crushing behavior of a natural seahorse tail), exhibiting a response that is stiffer, stronger, and more resilient than its cylindrical counterpart, whose plates translate and rotate on impact.

ON OUR WEB SITE

Read the full article at http://dx.doi.org/10.1126/science.aaa6683

CONCLUSION: Exploration of these biologically inspired designs provides insight into the mechanical benefits for seahorses to have evolved prehensile tails composed of armored plates organized into square prisms. Beyond their intended practical applications, engineering designs are convenient means to answer elusive biological questions when live animal data are unavailable (for example, seahorses do not have cylindrical tails). Understanding the role of mechanics in these prototypes may help engineers to develop future seahorse-inspired technologies that mimic the prehensile and armored functions of the natural appendage for a variety of applications in robotics, defense systems, or biomedicine. ■

The list of author affiliations is available in the full article online.
*Corresponding author. E-mail: mmporte@clemson.edu
Cite this article as M. M. Porter *et al.*, *Science* **349**, aaa6683 (2015). DOI: 10.1126/science.aaa6683

RESEARCH ARTICLE

BIOMECHANICS

Why the seahorse tail is square

Michael M. Porter,[1]* Dominique Adriaens,[2] Ross L. Hatton,[3] Marc A. Meyers,[4,5,6] Joanna McKittrick[4,5]

Whereas the predominant shapes of most animal tails are cylindrical, seahorse tails are square prisms. Seahorses use their tails as flexible grasping appendages, in spite of a rigid bony armor that fully encases their bodies. We explore the mechanics of two three-dimensional–printed models that mimic either the natural (square prism) or hypothetical (cylindrical) architecture of a seahorse tail to uncover whether or not the square geometry provides any functional advantages. Our results show that the square prism is more resilient when crushed and provides a mechanism for preserving articulatory organization upon extensive bending and twisting, as compared with its cylindrical counterpart. Thus, the square architecture is better than the circular one in the context of two integrated functions: grasping ability and crushing resistance.

Seahorses do not use their tails for swimming because they lack a caudal fin (*1*), but instead as flexible prehensile appendages that allow them to hide and rely on body crypsis to evade predators (*2*) and capture prey (*3*) by holding on to objects such as sea grasses, mangrove roots, and coral reefs (*4*). The skeleton of a seahorse consists of a rigid, subdermal armor of articulating bony plates, formed within the skin, that fully encase its body (Fig. 1A) (*5*–*13*). The tail armor is arranged into several ring-like segments composed of four L-shaped plates that surround a central vertebra (Fig. 1B). Muscles attached to the vertebrae transmit forces to the bony plates to control motion (*10*–*12*). Recent studies on the musculoskeletal structure, biomechanics, and kinematics of seahorse tails suggest that this bony-plated armor actively facilitates tail bending and twisting (Fig. 1B) (*10*–*12*) as well as resists vertebral fracture due to impact and crushing (Fig. 1C) (*13*). Selective pressures related to the defensive strategies [bony plates make eating seahorses difficult (*2*)] and feeding behavior [tail-attached, sit-and-wait suction feeding (*3*)] of seahorses may have driven the evolution of an ancestral plated system (square in cross section, but rather rigid and nonprehensile) into a more flexible system of similar plate organization for an added grasping functionality. Accordingly, we hypothesize that the cross-sectional square architecture of a seahorse tail possesses several mechanical advantages that could have helped promote this adaptation, especially when compared with other grasping appendages in unrelated animal species and other plated (nonsquare) skeletons in unrelated fish species.

Whereas several animals have developed grasping appendages that are cylindrical and composed of soft tissues surrounding a central axis of articulating skeletal elements (for example, tails of New World monkeys and some lizards, salamanders, marsupials, and rodents) (*14*–*17*), a peripherally plated skeleton is not exclusive to fishes and is even an ancestral condition of the vertebral lineages (*18*, *19*), with different patterns having arisen independently (such as ostracoderms, polypterids, gasterosteids, loricariids, and pegasids) (*20*). One recurrent pattern is where consecutive plates articulate through a peg-and-socket connection, combining some level of flexibility with strength. Such a joint is also present in seahorses, as well as closely related species from the same family of Syngnathidae (pipehorses, pipefishes, and seadragons). What differs among them, however, is that there is notable variation in the size of pegs and shape of sockets, as has recently been observed (*12*). The ancestral syngnathid configuration is a rather rigid nonprehensile tail that is completely enclosed by strongly abutting but articulating (peg-and-socket) bony plates, such as those found in pipefishes (*12*). Seahorses and pipehorses are the only lineages that use their tails as prehensile organs. Yet, they share with other syngnathids, and closely related seamoths (Pegasidae), a similar tail cross section that is not ovally shaped (as would be expected for fishes), but approximately square (*5*–*13*). Because the latter (pipefishes, seadragons, and seamoths) do not have flexible tails, this suggests that the square morphology may not reflect a structural adaptation directly related to tail prehensility but could provide some form of protection. Although it is likely that larger fish may swallow seahorses and other syngnathids whole, the peripherally plated

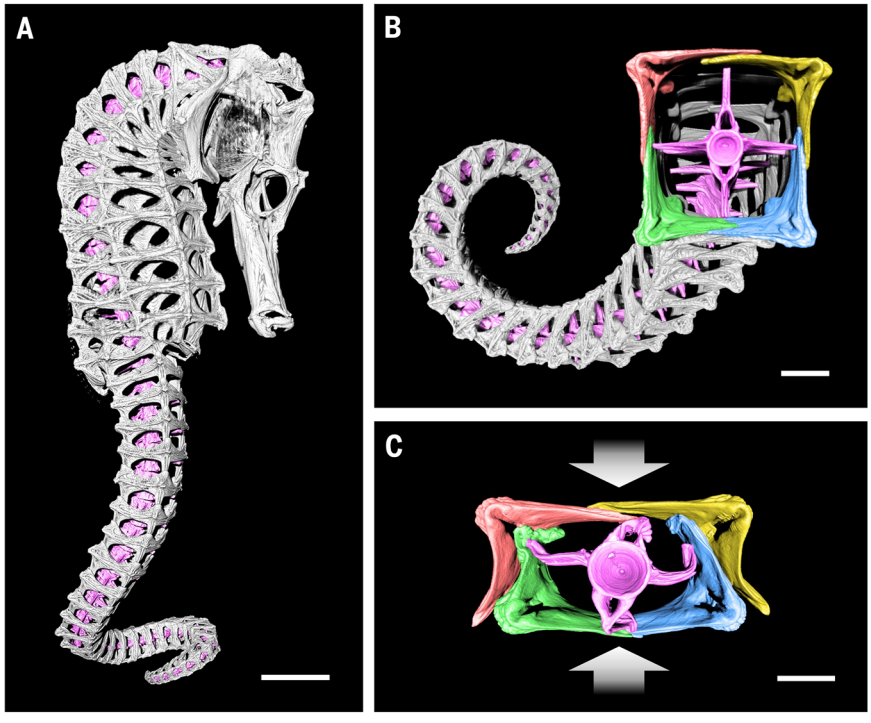

Fig. 1. Seahorse skeletons are composed of highly articulated bony plates that surround a central vertebral column. (**A** and **B**) μCT images of (A) a seahorse skeleton (*H. reidi*) and (B) its tail, illustrating its square cross section and particular flexibility. (**C**) μCT image of a seahorse tail segment (*H. kuda*) after crushing up to ~60% of its original height. For visual clarity, the vertebrae are color-masked magenta, and the bony plates are color-masked red, yellow, blue, and green. Scale bars, (A) 10 mm; (B) and (C) 2 mm.

[1]Department of Mechanical Engineering, Clemson University, Clemson, SC 29634, USA. [2]Evolutionary Morphology of Vertebrates, Ghent University, K.L. Ledeganckstraat 35, B-9000 Ghent, Belgium. [3]School of Mechanical, Industrial, and Manufacturing Engineering, Oregon State University, Corvallis, OR 97330, USA. [4]Materials Science and Engineering Program, University of California, San Diego, La Jolla, CA 92093, USA. [5]Department of Mechanical and Aerospace Engineering, University of California, San Diego, La Jolla, CA 92093, USA. [6]Department of NanoEngineering, University of California, San Diego, La Jolla, CA 92093, USA.
*Corresponding author. E-mail: mmporte@clemson.edu

skeleton can protect their soft tissues against bites from smaller predators (*13*). In the case of pipefishes, which closely resemble the syngnathid ancestral state, fortifying the body as a poorly bendable "stick" makes them difficult prey to swallow and digest (*2*). Also, their second largest group of predators (next to teleosts) are waterbirds, with waders and seabirds accounting for 32% of all syngnathid predators (*2*). Because many birds use beaks to clamp down and capture prey before feeding, it is likely that the skeletal armor could protect seahorses from crushing (*13*). When a seahorse tail is crushed, for instance, the bony plates slide past one another, acting as an energy absorption mechanism, which resists fracture of the vertebral column (Fig. 1C) (*13*). This is different from the mechanisms observed in the skin and scales of other fish that provide an optimal flexural stiffness for both swimming and protection against predatory attacks (*21*–*23*). Hence, this complex skeletal system may provide seahorses an advantageous combination of joint flexibility for prehension with shielding from external forces for protection.

Similar to recent works that used robots to investigate animal behavior and locomotion (*24*, *25*), we used three-dimensional (3D)–printed models to explore the mechanics of seahorse tails. Because cylindrical seahorse tails do not exist in nature, 3D printing allows us to build functional models of this hypothetical system so as to investigate what mechanical advantages an articulated square prism may have over a cylinder, which is the common shape of most other animal tails. This falsifiable methodology is particularly useful to examine the mechanics of musculoskeletal systems in vertebrates that are difficult or impossible to study in nature (for example, seahorses do not have cylindrical tails). Thus, via 3D printing we replicated comparative models that mimic the specialized joints and complex morphologies of both the natural (square prism) and hypothetical (cylindrical) systems.

In a quest to better understand armored prehensility in seahorses and develop useful tools inspired by their tails, we designed this new class of highly articulated structures—not only for biological research, but also for a wide range of potential robotics, armored systems, and biomedical applications. Such applications for the seahorse-inspired technology would be able to take advantage of a large body of kinematics and actuation work that has been developed for similar long, slender "continuum" structures inspired by organisms such as snakes and worms (*26*–*30*), squids and octopuses (tentacles) (*31*, *32*), elephants (trunks) (*33*), and plants (tendrils and roots) (*34*, *35*). The combination of articulated rigid plates and elastic deformability observed in a seahorse tail (Fig. 1) could strike a promising balance between the two dominant paradigms in robotics design: being lighter and more compliant than traditional "hard" robots built from servos and metal, but more robust and resistant to external tractions than the emerging class of "soft" robots with silicone-membrane bodies. However, akin to nature, the vast majority of these serially articulated structures (*26*–*35*) have cylindrical profiles. Therefore, we ask the question, why might square prisms be better than cylinders?

Inspired by seahorses, designed by engineers

Seahorse tails predominantly bend ventrally (*7*), an adaptation that allows seahorses to grasp objects in front of their line of sight. However, seahorses can also hyperextend and twist their tails to achieve moderate degrees of bending in the dorsal and lateral directions. Measuring the angle of tail rotation of a seahorse (*Hippocampus kuda*) shows that the tail can bend ~850° ventrally, ~290° dorsally, and ~570° laterally, whereas concurrent bending and twisting allows the tail to bend in the dorsal or lateral directions to nearly the same degree as in pure ventral bending (Fig. 2A). Although tail movement is primarily controlled by the epaxial, hypaxial, and ventral intervertebral muscles, and constrained by the vertebral connections and segment interlocks (*7*, *10*, *12*), three additional morphological features present in the skeletal armor also influence tail bending (Fig. 2, B and C): (i) plate size, (ii) plate skew, and (iii) plate overlapping.

Recently, Praet *et al.* (*10*) measured the size and skewing of the bony plates along the length of a seahorse tail. The plates, and consequently the segments, decrease in size from the proximal to distal end of the tail; the resulting finer articulation enables a seahorse to smoothly bend its tail into a logarithmic spiral, with increasing curvature toward the tip (*10*). The plate skew [measured as the angle θ between the midline of the lateral plates and a normal vector to the central spinal column (Fig. 2B)] increases linearly along the length of the tail, so that the lateral plates and the spinal column are nearly orthogonal (θ = ~0°) at the proximal base, while highly skewed (θ = ~45°) at the distal tip (*10*). On the basis of a 2D geometric model of the tail kinematics that reduces the segment joints to their key salient features [two peg-and-socket joints that rotate about a single ball-and-socket joint (fig. S2C)], we identified two primary mechanisms by which the skew of the tail segments produces a bias toward ventral bending over dorsal bending (*36*): (i) The ventral plates are shifted proximally (toward the trunk), whereas the dorsal plates are shifted distally (away from the trunk). This proximal-distal shift changes the position of the pegs within the sockets when the tail is in a straightened position, so that the pegs are centered in the sockets on the ventral side but positioned increasingly closer to the distal-most end of the sockets on the dorsal side (fig. S2). This offset placement limits the range of motion of these joints in dorsal bending while increasing their range in ventral bending. (ii) Distally shifting the dorsal peg-and-socket joints angles them toward the ventral surface, so that they remain tangent to the rotation of the ball-and-socket joint (fig. S2). During ventral bending, this offset inclination

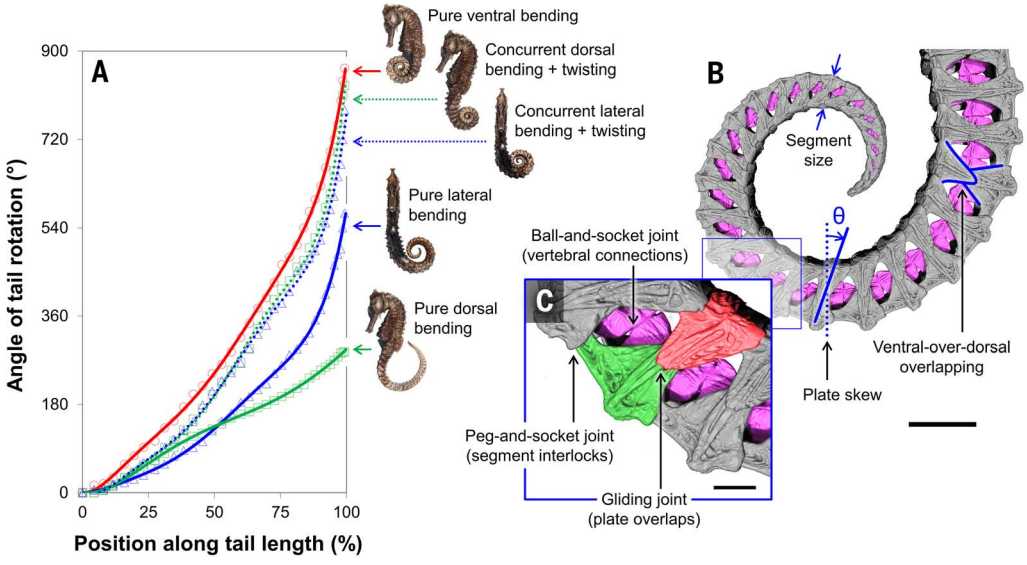

Fig. 2. Seahorse tails predominantly bend ventrally into a logarithmic spiral. (**A**) Plot of the angle of rotation of a seahorse tail (*H. kuda*) from the proximal base (0%) to the distal tip (100%) of the tail in different bending orientations. (**B** and **C**) μCT images of a seahorse tail (*H. reidi*) bent in the ventral direction, illustrating (B) the segment size, plate skew, and ventral-over-dorsal overlapping features, and (C) the ball-and-socket, peg-and-socket, and gliding joints. For visual clarity, the vertebral column is color-masked magenta, and the dorsal and ventral plates are color-masked green and red, respectively. Scale bars, (B) 6 mm; (C) 1.5 mm.

allows the sockets of the distal plates to lie flush with the pegs of the proximal plates on the dorsal side of the tail, instead of "peeling" away at these joints. These two mechanisms both increase the range of motion of the joints in the ventral direction, producing the different sagittal (ventro-dorsal) bend angles observed in Fig. 2A, and improve the alignment of adjacent plates when the tail is in a curled position (Fig. 2B). Further, it was previously noted that the ventral plates always overlap the dorsal plates along the lateral sides of the tail (Fig. 2B) (*13*). This bisymmetric ventral-over-dorsal overlapping arrangement likely promotes ventral tail bending as well (fig. S3), so that the ventral plates have more freedom to slide and rotate, and hence more articulation space, because they are not rigidly attached to the vertebral column [as in the case of the dorsal plates (*7*, *10*)]. Consequently, we hypothesize that eliminating all of these morphological features (plate size, skew, and ventral-over-dorsal overlaps) from the skeletal armor of a seahorse would allow its tail to bend equally in all directions (ignoring the effect of muscular orientation and connective tissue composition).

To test this hypothesis, we designed and built two artificial skeletons composed of articulating plates and vertebrae arranged into either the natural square prism or a hypothetical cylindrical architecture (*36*). In Fig. 3, microcomputed tomography (μCT) images of three segments of a natural seahorse tail skeleton are juxtaposed with computer-aided design (CAD) models generated to fabricate the 3D-printed prototypes. Pictures of the two prototypes are shown in Fig. 4, highlighting the key structural elements incorporated into the designs. The primary components of the prototypes were scaled up and modified via CAD software (SolidWorks, Dassault Systemes, Waltham, MA) by mimicking the dominant geometries observed from μCT scans of a natural bony plate and vertebra extracted from the proximal base of a seahorse tail. The computer models were then transferred to a 3D printer (Dimension 1200es, Stratasys, Eden Prairie, MN) to build the artificial plates and vertebrae from a rigid thermoplastic [ABS*plus* (Stratasys), where both the black and blue materials have nearly equivalent properties, with a compressive modulus of ~700 MPa], which were assembled together with compression springs (with a spring constant of 3.36 N/mm) and elastic bands (with a tensile modulus of 15 MPa) (Fig. 4 and table S1). The materials selected for the different components of the prototypes were chosen for convenience (ABS*plus* is available in-house, and the elastic bands are available at local retailers) and showed a similar order-of-magnitude difference in stiffness to that observed in natural fish bones (3.5 to 19.4 GPa) (*37*) and fibrous tissues (1.2 to 10 MPa) (*37*), respectively (table S1). The compression springs were selected to mimic the highly deformable compressive behavior observed in the vertebral struts of a natural seahorse tail [more detail is available in (*13*)]. Because the 3D-printed plates and vertebrae are nearly two orders of magnitude stiffer than the other load-bearing components (springs and elastic bands), they are approximated as fully rigid bodies throughout this study. Thus, the small volumetric differences between the "square" and "circular" plates can be considered negligible because the artificial plates and vertebrae are assumed to experience deformations much smaller than those observed in the overall structures (*36*).

In addition, both prototypes have three primary joints: ball-and-socket, peg-and-socket, and gliding (Fig. 4). These specialized joints provide the prototypes several internal degrees of rotational and translational freedom, allowing the structures to bend, twist, and compress with multiple modes of deformation. In building the prototypes, we excluded two features of the natural tail morphology: the tapering of the segments toward the distal end of the tail, and the

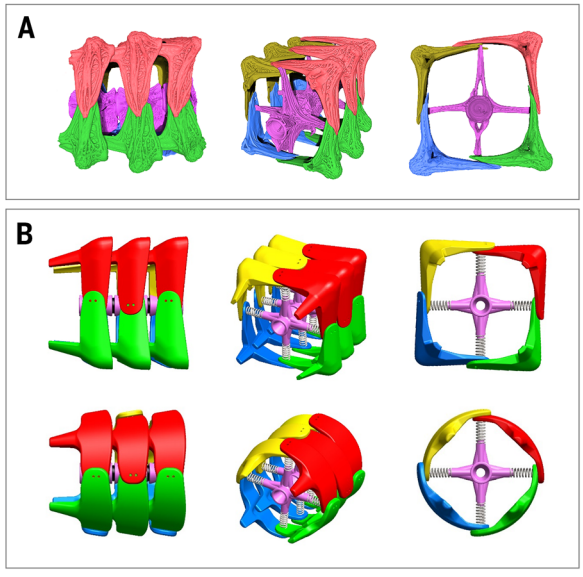

Fig. 3. Computer models designed to mimic the structural organization of a seahorse tail. (**A**) μCT images of a seahorse tail skeleton (*H. kuda*) composed of three segments. (**B**) CAD models of three segments from both the square prism (top) and cylindrical (bottom) artificial skeletons. For visual clarity, the vertebrae are color-masked magenta, and the plates are color-masked yellow, red, green, and blue.

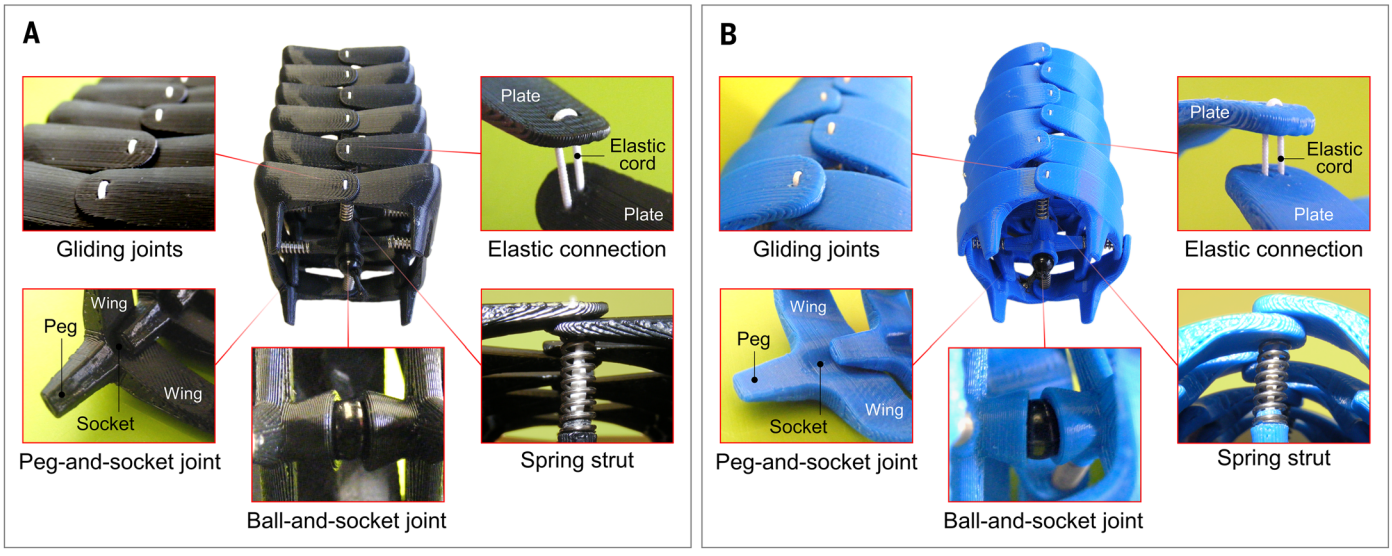

Fig. 4. 3D-printed prototypes designed to mimic the specialized joints of a seahorse tail. (**A** and **B**) Images of the seahorse-inspired prototypes with (A) a square cross section and (B) a circular cross section, depicting the primary structural features and joints incorporated into the designs.

skewing of the segments. This simplification focuses attention on the cross-sectional structure of the plates. The tapering is relatively small [<5% size difference between adjacent links near the proximal base (*10*)] and allows the tail to grasp small objects (*10*, *11*). Similarly, the change in segment skew is relatively small (~2° to 3° angular difference between adjacent links) and can be accounted for in the tail's bias toward ventral bending (fig. S2). If we had incorporated the segment skew in our model, we anticipate that the resulting offset between the ventral and dorsal plates would have provided a small increase to the crushing resistance of the prototypes (by spreading loads applied to a ventral plate across two dorsal plates, and vice versa). The sequence of intrasegmental connections (plate overlaps) in the prototypes was asymmetrically alternated, so that each alternating segment contains right-over-left overlaps, followed by left-over-right overlaps, along the central midlines, eliminating the regular ventral-over-dorsal overlapping arrangement observed in the natural tail. These design modifications produced a quadraxial symmetry in both prototypes, which as hypothesized facilitates equal bending in all three directions (ventral, dorsal, and lateral).

Bending, twisting, and prehension

The images and CAD models of the square prismatic and cylindrical prototypes shown in Fig. 5 illustrate the limits of bending and twisting, which would likely change by altering the size and skewing of the plates (*36*). If the plates are bisymmetrically overlapped to more closely mimic the natural configuration, the prototypes favor bending in the "ventral" direction, which was confirmed via experimental observations (fig. S3). Regardless, for comparative purposes, bending is primarily constrained by the ball-and-socket joints, which are designed to have a maximum rotation angle of ~12° in all directions (ignoring contact between the plates of adjacent segments). According to this constraint and as seen in Fig. 5, C and D, both artificial skeletons can bend ~90° over a span of approximately eight segments, matching that of the proximal base of a seahorse tail (*12*). When considering contact between the plates of adjacent segments, however, bending is slightly less restricted in the cylindrical prototype than in the square one. As shown in movie S1 and Fig. 5B, the cylindrical prototype can bend to nearly the same degree in any plane off-axis from the vertebral struts (covering all 360° of rotation), whereas the square prototype can bend to a higher degree in the planes oriented parallel and perpendicular to the vertebral struts (in the ventral-dorsal and lateral directions) than those off-axis because contact at the peg-and-socket joints restricts substantial out-of-plane bending.

Twisting, on the other hand, is fully constrained by the physical boundaries imposed at each peg-and-socket joint. As seen in Fig. 5, C and D, the overall twist of the cylindrical prototype is approximately twice that of the square prototype, with an angle of twist of ~30°—as opposed to only ~15°—between adjacent segments. This difference is due to the type of interference that occurs at the peg-and-socket joints. In the cylindrical prototype, interference between the pegs and vertebral struts limits twisting (Fig. 5D). However, in the square prototype, interference between the pegs and sockets occurs well before contact with the vertebral struts, restricting excessive torsion between segments (Fig. 5C).

This natural geometric constraint imposed by the peg-and-socket joints of the square architecture could help preserve musculoskeletal organization in a seahorse tail because it provides a natural safety factor against possible torsion-induced damage or misalignment from overtwisting. It also provides a passive mechanism for articulatory reorganization upon extensive bending and twisting, which could be advantageous for seahorses to expend less energy when returning their tails to a neutral resting position—slightly bent in the ventral direction (a result of skewing), but straight in the lateral directions [based on observations of a sedated seahorse (*11*)]. This mechanism observed in the square prototype is demonstrated in movie S1. After deformation, the square prototype always returns to the same linearly aligned resting position, whereas the cylindrical one does not (movie S1, dashed yellow lines). Instead, the lack of interference between its pegs and sockets allows the cylindrical prototype to rest in nearly any bent or twisted position.

In addition, the flat exterior surfaces of the square cross section increase contact area and stability when wrapped around an object, as compared with a circular cross section. When twisted, the square segments transform its exterior shape from a square prism to a solid helix, whereas the exterior profile of the cylindrical prototype remains unchanged under torsion (Fig. 5). The corner edges of this twisted configuration could provide the square architecture more prehensile control—for instance, when a seahorse adjusts its tail-grip on objects. Although not yet observed in nature, this type of twisted shape transformation could also be used to generate a sequence of repetitive forces allowing the articulated square prism to move or wriggle along a variety of substrates in a traveling-coil motion, akin to that demonstrated in modular snake robots (*38*). Thus, the flattened topology of the square architecture has several functional advantages related to bending

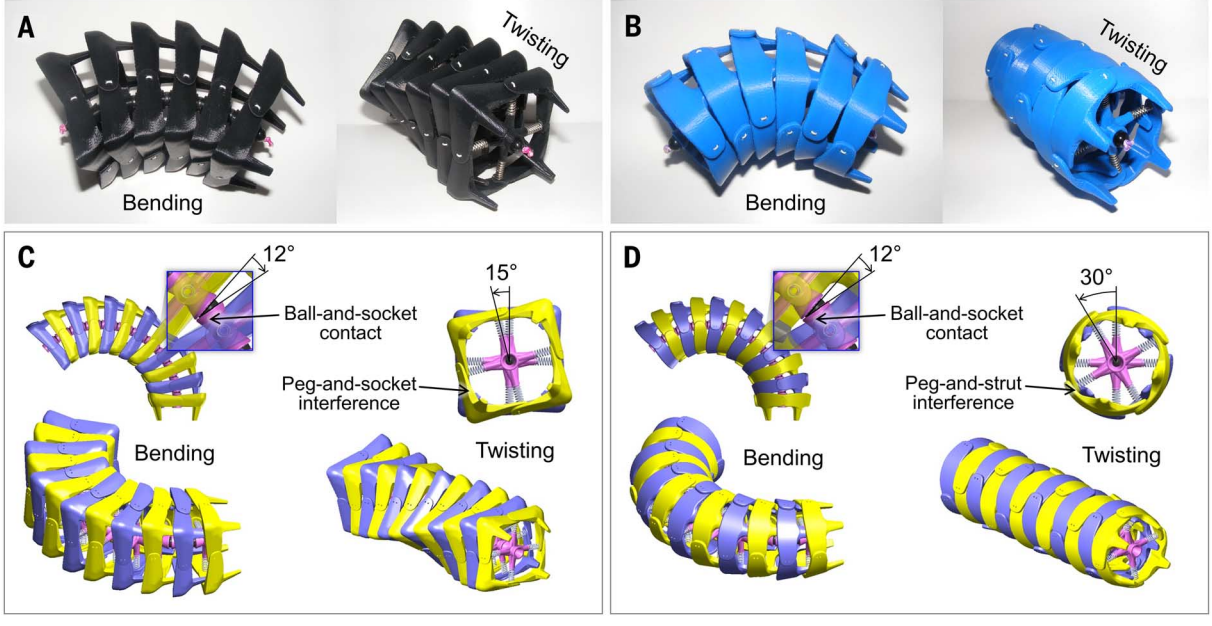

Fig. 5. Bending and twisting performance of the prototypes. (**A** and **B**) Photographs and (**C** and **D**) CAD models of the square (left) and cylindrical (right) prototypes, illustrating the limits of bending and twisting. A more complete comparison of bending and twisting is provided in movie S1.

and twisting that could allow seahorses to grasp objects with more control.

Impact, crushing, and protection

Beyond simple bending and twisting, the artificial skeletons also mimic the protective energy absorption mechanism observed in the highly deformable skeleton of a seahorse tail (Fig. 1C) (*13*). When subject to impact, such as the compressive force of a rubber mallet (Fig. 6, A and B, and movie S2), the gliding joints and vertebral struts of the prototypes allow the plates to slide past one another (or rotate, in the case of the cylindrical prototype), absorb the impact when compressed, and subsequently protect the internal vertebral column from brittle fracture. As seen in movie S2, the square prototype returns to its linearly aligned resting position after impact, whereas the cylindrical one remains partially deformed and misaligned (even when the first and last segments are taped to the supporting plane). Although there is some plate rotation observed in segments of the square prototype adjacent to the primary impact point, the plates directly impacted mainly show linear sliding. In contrast, the cylindrical prototype experiences extreme reverberations transferred through its vertebral column upon impact.

Under ideal uniaxial compression, the artificial square skeleton deforms linearly by sliding its plates past one another with approximately one degree of translational freedom (Fig. 6C). The cylindrical skeleton, on the other hand, deforms with approximately two degrees of freedom (one translational and one rotational), resulting in linear compressive and expansive deformations parallel and perpendicular to the applied force, respectively, leading to a cross-sectional shape change from circular to elliptical (Fig. 6D). When subject to biaxial compression, both the square and cylindrical skeletons deform bisymmetrically. However, the square architecture can contract its outer profile by ~30% (apparent reduction of cross-sectional area) (Fig. 6E), whereas the contracted profile of the circular one is reduced by only ~10% (Fig. 6F). The difference in the compressive behavior of the two cross sections is a result of the different plate geometries. The flattened morphology of the plates in the square skeleton allows linear sliding to occur without disrupting its outer profile, whereas the rounded plates in the circular one interfere and create large gaps or rotation between adjacent plates. Although seahorses are unlikely to experience biaxial compression in nature, this type of contractive deformation is of interest for comparison to similar behaviors that occur in other organisms and mimetic technologies (such as peristalsis and burrowing) (*29*, *39*).

In contrast, the mechanical behavior of square and circular solid rings (without gliding joints) subject to transverse uniaxial and transverse biaxial compression is shown to the right of each image in Fig. 6, C to F (where the resulting deformations are exaggerated for clarity). Derivations of analytical expressions describing these shapes, shown in figs. S4 and S5, are included in (*36*). Under transverse uniaxial compression, thin solid rings buckle at their midsections when the internal stresses accumulated in the rings exceed the yield stress of the ring material, forming plastic yield hinges where permanent deformation begins (Fig. 6, C and D) (*40*–*42*). By analogy, rings subject to biaxial compression also form plastic hinges at the locations of maximum stress where yielding begins (Fig. 6, E and F, red dots). The onset of these plastic hinges occurs when the absolute internal moment ($|M'|$) accumulated in the rings exceeds the plastic yield moment of the ring material (M_0), which are both approximated as a moments per unit length (b) for square and circular rings (*40*–*42*)

$$|M'| > M_0 = \frac{\sigma_0 t^2}{4} \qquad (1)$$

where σ_0 is the yield strength of the ring material and t is the ring thickness, assuming plane strain so that the length of the ring (or tube) is much greater than its thickness ($b >> t$). The locations of the plastic hinge zones are shown in fig. S6, determined analytically in (*36*), and verified experimentally for unilateral compression in Fig. 7, F and G. Accordingly, the plastic hinge zones are assumed to be controlled by the tensile properties of the ring material (*36*), as noted by the observation of crazing that occurs because of tension at these locations (Fig. 7, F and G).

In seahorses, the problem of plastic hinge formation and subsequent buckling of their ring-like armor is solved by having gliding joints at the locations of these plastic yield zones. The highly deformable vertebral struts and connective tissues—which exhibit local buckling and tensile stretching rather than brittle fracture and tearing, respectively—let the bony plates slide past one another to absorb energy when compressed (Fig. 1C) (*13*). This mechanism allows the tail (of a deceased seahorse) to deform to nearly 50% before the onset of permanent failure in the vertebral column (*13*). Exploiting this mechanism, we mimicked the vertebral struts and connective collagen with compression springs and elastic bands, respectively. When crushed, the springs compress—and bend or buckle, if necessary—to allow the artificial plates to slide and/or rotate (Fig. 7, B and C, and movie S2). As the plates move, the elastic bands connecting adjacent plates stretch, a response observed to be independent of the displacement rate (fig. S1). These two mechanisms bear the load in the two prototypes when subjected to transverse compression, exhibiting up to ~17% linear elastic deformation in the square prototype and ~12% in the circular one (Fig. 7A).

Upon further analysis, it is apparent that the square prototype under compression is stiffer, stronger, and more resilient than the circular one (Fig. 7A). The load carried by the square skeleton composed of six segments ($P_{\square}$) can be expressed as a function of its linear displacement (δ), treating

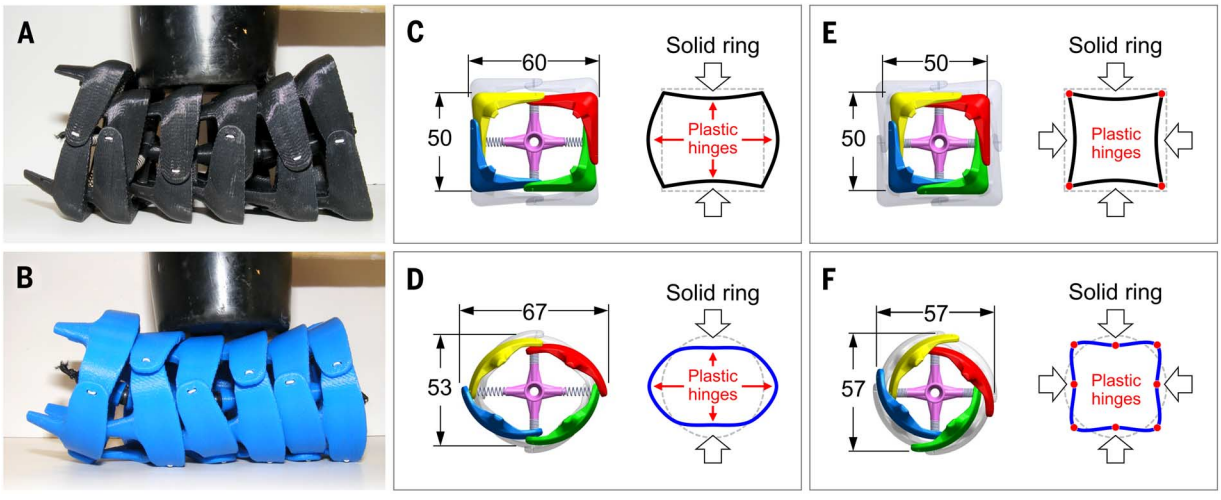

Fig. 6. Impact and crushing performance of the prototypes. (**A** and **B**) Images of the square (top) and cylindrical (bottom) prototypes subject to impact by a rubber mallet. A high-speed comparison of the prototypes subject to impact is provided in movie S2. (**C** to **F**) CAD models of the artificial skeletons (left) and representative schematics of solid rings (right) subject to transverse uniaxial and transverse biaxial compression, showing the locations of primary and secondary plastic hinges with red arrows in (C) and (D) and red dots in (E) and (F). All units are in millimeters.

the 3D-printed plates and vertebrae as rigid bodies, so that

$$P_{\square} = 6 \times \left(\frac{1}{2}k_s + 6\frac{\beta_s}{L_s^3} + 4k_e\right)\delta \qquad (2)$$

where k_s = 3.36 N/mm is the compressive spring constant, $\beta_s = 2.0 \times 10^{-4}$ N · m^2 is the flexural rigidity of the springs, L_s = 10 mm is the active length of the springs in bending, and k_e = 0.20 N/mm is the effective spring constant of the elastic bands (fig. S7) (*36*). Similarly, the load carried by the cylindrical skeleton composed of six segments ($P_{\circ}$) can also be expressed as a function of its linear displacement (δ)

$$P_{\circ} = 6 \times \left(\frac{1}{4}k_s(\delta+\gamma)\frac{a}{c} + k_e\zeta\frac{b}{c}\right) \qquad (3)$$

where a, b, and c are geometric relations dependent on the radius of plate curvature (R = 30 mm), and (δ + γ) and ζ are the vertical and lateral displacements of the cylindrical skeleton, respectively (*36*). To account for the six segments in each prototype compressed in parallel (Fig. 7, A to C), Eqs. 2 and 3 are both multiplied by a factor of six.

A plot of these equations (dashed lines) is shown in Fig. 7A, compared with experimental data obtained via compression tests of the prototypes (Fig. 7A, solid lines), each composed of six segments. The analytical expressions ($P_{\square}$ and $P_{\circ}$) both underpredict the actual load carried by the two prototypes. This discrepancy is because for simplicity, the frictional forces between adjacent plates and the prototypes with the compression platforms were neglected throughout the analyses. Regardless, the force-displacement curves in Fig. 7A illustrate the fact that the square prototype is ~3× stiffer, ~4× stronger, and ~1.5× more elastic than its circular counterpart. At the point at which the load drops off because of a minor collapse of the structures (Fig. 7A, red arrows), the springs are almost fully compressed and begin to buckle before disjoining from the plates. At this point, the prototypes no longer exhibit a purely elastic behavior. Although recoverable, the structural integrity of the internal struts (compression springs) becomes compromised, making these points the elastic limits of the prototypes.

In juxtaposition, the compressive behavior of square and circular solid rings composed of the same 3D-print material (ABS*plus*) used to fabricate the seahorse-inspired prototypes is shown in Fig. 7, D to G. As seen in the plot of Fig. 7D, the solid rings are seemingly much stronger and stiffer than the articulated prototypes (Fig. 7A). Also, the square ring is an order of magnitude stiffer and stronger than the circular one of equal height but undergoes much less transverse

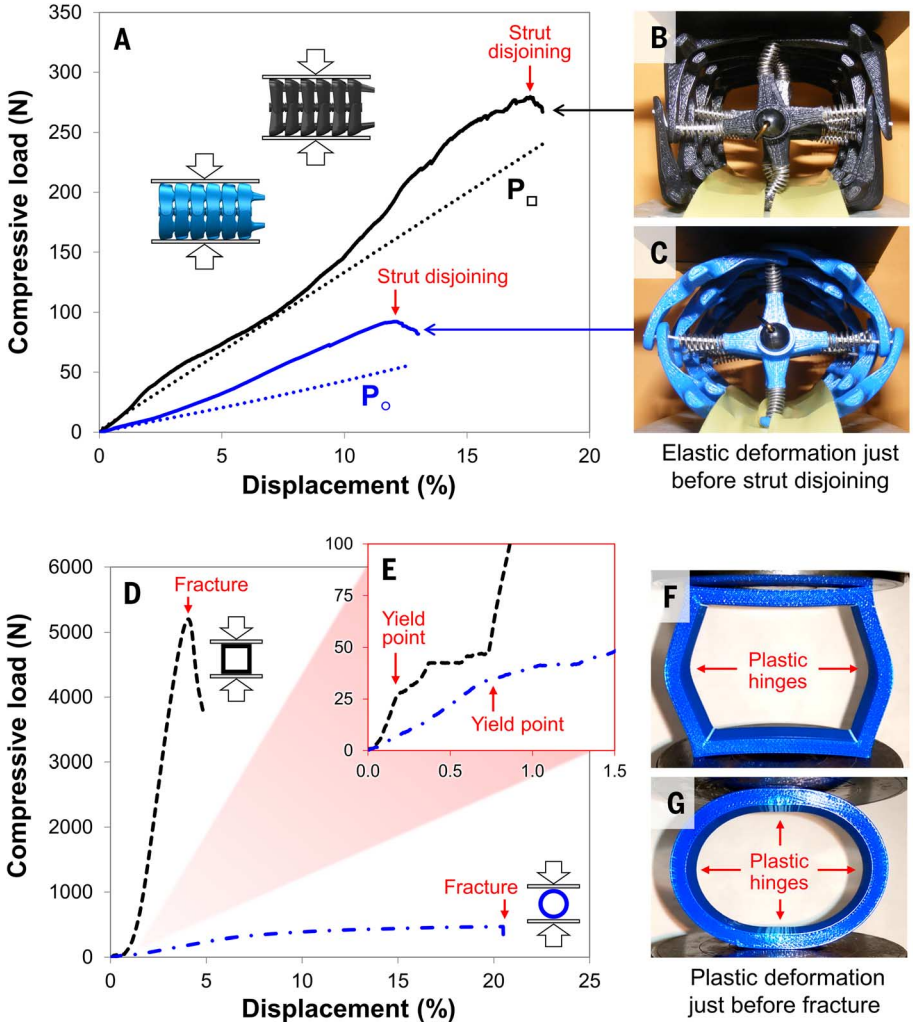

Fig. 7. Unilateral compression of the prototypes and solid rings. (**A**) Plot of the compressive load versus normalized displacement for the square (black) and cylindrical (blue) prototypes subject to unilateral compression between two rigid plates. The solid lines correspond to direct experimental measurements, and the dashed lines correspond to theoretical predictions of load and displacement from Eqs. 2 and 3. (**B** and **C**) Images of the square (top) and cylindrical (bottom) prototypes subject to transverse unilateral compression just before strut disjoining, corresponding to the red arrows in (A). (**D**) Plot of the compressive load versus normalized displacement for a square (black dashed line) and circular (blue dashed-dotted line) solid ring subject to transverse unilateral compression between two rigid plates. (**E**) Magnified plot illustrating the elastic region and yield points of the load-displacement curves in (D). (**F** and **G**) Images of the square (top) and circular (bottom) solid rings subject to transverse unilateral compression just before fracture, corresponding to the red arrows in (D).

displacement before failure. Nevertheless, these behaviors (Fig. 7D) occur when the solid rings are loaded within the plastic regime, beyond the initial formation of plastic hinges [which begin at the yield point, the first sign of permanent deformation (Fig. 7E)]. Considering this, it is more useful to compare the elastic behavior of the articulated prototypes (Fig. 7A) with that of the solid rings (Fig. 7E). As indicated in Fig. 7E, both solid rings begin to yield at ~30 N, whereas the square ring elastically deforms only ~0.1% and the circular ring ~0.8%. When crushed, the square prototype outperforms the cylindrical one, exhibiting a higher strength and stiffness, analogous to the mechanical performance of the solid rings. The square prototype is also more resilient than the cylindrical one, absorbing more energy before failure (strut disjoining), a trend not observed in the solid rings (solid rings with circular cross sections are more resilient than square ones). Thus, the specialized joints present in the prototypes (and likewise in a seahorse tail) provide the structures an enhanced range of motion, not only in bending and twisting but also in resistance to crushing.

Concluding remarks

The highly articulated bony plates that surround the central vertebral axis of a seahorse tail actively facilitate bending and twisting as well as resist vertebral fracture from impact and crushing. To explore why the bony plates are arranged into cross-sectional squares rather than circles, we analyzed the mechanics of 3D-printed models that mimic the natural (square prism) and hypothetical (cylindrical) architectures of a seahorse tail skeleton. Physical manipulation of the two prototypes revealed that the square architecture possesses several mechanical advantages over its circular counterpart in bending, twisting, and resistance to crushing. The enhanced performance realized in the square architecture provides insight into the way in which seahorses may benefit from having prehensile tails composed of armored plates organized into square prisms, rather than cylinders. This study demonstrates that engineering designs are convenient means to answer elusive biological questions when biological data are nonexistent or difficult to obtain. In addition, understanding the role of mechanics in these biologically inspired designs may help engineers to develop seahorse-inspired technologies for a variety of applications in robotics, defense systems, or biomedicine.

REFERENCES AND NOTES

1. M. A. Ashley-Ross, Mechanical properties of the dorsal fin muscle of seahorse (*Hippocampus*) and pipefish (*Syngnathus*). *J. Exp. Zool.* **293**, 561–577 (2002). doi: 10.1002/jez.10183; pmid: 12410605
2. D. Kleiber, L. K. Blight, I. R. Caldwell, A. C. J. Vincent, The importance of seahorses and pipefishes in the diet of marine animals. *Rev. Fish Biol. Fish.* **21**, 205–223 (2011). doi: 10.1007/s11160-010-9167-5
3. S. Van Wassenbergh, G. Roos, L. Ferry, An adaptive explanation for the horse-like shape of seahorses. *Nat. Commun.* **2**, 164 (2011). doi: 10.1038/ncomms1168; pmid: 21266964
4. S. A. Lourie, S. J. Foster, E. W. T. Cooper, A. C. J. Vincent, *A Guide to the Identification of Seahorses* (Project Seahorse, Washington, DC, 2004).
5. R. Anthony, L. Chevroton, Considérations sur les attitudes et la locomotion de l'hippocampe, étude chronophotographique. *Arch. Zool. Exp. Gen.* **51**, 11–22 (1913).
6. H. Peters, [On the ecologic physiology of the sea horse (*Hippocampus brevirostris*)]. *Z. Vgl. Physiol.* **33**, 207–265 (1951). doi: 10.1007/BF00395584; pmid: 24541372
7. M. E. Hale, Functional morphology of ventral tail bending and prehensile abilities of the seahorse, *Hippocampus kuda*. *J. Morphol.* **227**, 51–65 (1996). doi: 10.1002/(SICI)1097-4687(199601)227:1<51::AID-JMOR4>3.0.CO;2-S
8. E. Bruner, V. Bartolino, Morphological variation in the seahorse vertebral system. *Int. J. Morphol.* **26**, 247–262 (2008). doi: 10.4067/S0717-95022008000200002
9. S. Van Cauter *et al*., Virtual design from nature: Kinematic modeling of the seahorse tail. *SIMULIA Customer Conference*, 770–783 (2010).
10. T. Praet *et al*., Inspiration from nature: Dynamic modelling of the musculoskeletal structure of the seahorse tail. *Int. J. Numer. Method Biomed. Eng.* **28**, 1028–1042 (2012). doi: 10.1002/cnm.2499; pmid: 23027633
11. T. Praet, thesis, Ghent University, Ghent, Belgium (2013).
12. C. Neutens *et al*., Grasping convergent evolution in syngnathids: A unique tale of tails. *J. Anat.* **224**, 710–723 (2014). doi: 10.1111/joa.12181; pmid: 24697519
13. M. M. Porter, E. Novitskaya, A. B. Castro-Ceseña, M. A. Meyers, J. McKittrick, Highly deformable bones: Unusual deformation mechanisms of seahorse armor. *Acta Biomater.* **9**, 6763–6770 (2013). doi: 10.1016/j.actbio.2013.02.045; pmid: 23470547
14. G. C. Hickman, The mammalian tail: A review of functions. *Mammal Rev.* **9**, 143–157 (1979). doi: 10.1111/j.1365-2907.1979.tb00252.x
15. L. Emmons, A. H. Gentry, Tropical forest structure and the distribution of gliding and prehensile-tailed vertebrates. *Am. Nat.* **121**, 513–524 (1983). doi: 10.1086/284079
16. K. C. Zippel, R. E. Glor, J. E. Bertram, On caudal prehensility and phylogenetic constraint in lizards: The influence of ancestral anatomy on function in Corucia and Furcifer. *J. Morphol.* **239**, 143–155 (1999). doi: 10.1002/(SICI)1097-4687(199902)239:2<143::AID-JMOR3>3.0.CO;2-O
17. J. M. Organ, V. B. Deleon, Q. Wang, T. D. Smith, From head to tail: New models and approaches in primate functional anatomy and biomechanics. *Anat. Rec.* **293**, 544–548 (2010). doi: 10.1002/ar.21132; pmid: 20235310
18. J.-Y. Sire, A. Huysseune, Formation of dermal skeletal and dental tissues in fish: A comparative and evolutionary approach. *Biol. Rev. Camb. Philos. Soc.* **78**, 219–249 (2003). doi: 10.1017/S1464793102006073; pmid: 12803422
19. P. C. J. Donoghue, I. J. Sansom, J. P. Downs, Early evolution of vertebrate skeletal tissues and cellular interactions, and the canalization of skeletal development. *J. Exp. Zoolog. B Mol. Dev. Evol.* **306**, 278–294 (2006). doi: 10.1002/jez.b.21090; pmid: 16555304
20. J. S. Nelson, *Fishes of the World* (Wiley, New York, 2006).
21. J. Long, M. Hale, M. Mchenry, M. Westneat, Functions of fish skin: Flexural stiffness and steady swimming of longnose gar, Lepisosteus osseus. *J. Exp. Biol.* **199**, 2139–2151 (1996). pmid: 9320050
22. B. J. F. Bruet, J. Song, M. C. Boyce, C. Ortiz, Materials design principles of ancient fish armour. *Nat. Mater.* **7**, 748–756 (2008). doi: 10.1038/nmat2231; pmid: 18660814
23. F. J. Vernerey, F. Barthelat, Skin and scales of teleost fish: Simple structure but high performance and multiple functions. *J. Mech. Phys. Solids* **68**, 66–76 (2014). doi: 10.1016/j.jmps.2014.01.005
24. T. Libby *et al*., Tail-assisted pitch control in lizards, robots and dinosaurs. *Nature* **481**, 181–184 (2012). doi: 10.1038/nature10710; pmid: 22217942
25. A. J. Ijspeert, Biorobotics: Using robots to emulate and investigate agile locomotion. *Science* **346**, 196–203 (2014). doi: 10.1126/science.1254486; pmid: 25301621
26. K. Xu, N. Simaan, Actuation compensation for flexible surgical snake-like robots with redundant remote actuation. *IEEE International Conference on Robotics and Automation*, 4148–4154 (2006).
27. C. Wright *et al*., Design of a modular snake robot. *IEEE/RSJ International Conference on Intelligent Robots and Systems* (2007).
28. J. K. Hopkins, B. W. Spranklin, S. K. Gupta, A survey of snake-inspired robot designs. *Bioinspir. Biomim.* **4**, 021001 (2009). doi: 10.1088/1748-3182/4/2/021001; pmid: 19158415
29. K. A. Daltorio *et al*., Efficient worm-like locomotion: Slip and control of soft-bodied peristaltic robots. *Bioinspir. Biomim.* **8**, 035003 (2013). doi: 10.1088/1748-3182/8/3/035003; pmid: 23981561
30. C. D. Onal, R. J. Wood, D. Rus, An origami-inspired approach to worm robots. *IEEE/ASME Trans. Mechatron.* **18**, 430–438 (2013). doi: 10.1109/TMECH.2012.2210239
31. I. D. Walker *et al*., Continuum robot arms inspired by cephalopods. *Conference on Unmanned Ground Vehicle Technology VII* **5804**, 303–314 (2005).
32. R. F. Shepherd *et al*., Multigait soft robot. *Proc. Natl. Acad. Sci. U.S.A.* **108**, 20400–20403 (2011). doi: 10.1073/pnas.1116564108; pmid: 22123978
33. I. D. Walker, M. W. Hannan, A novel 'elephant's trunk' robot. *IEEE/ASME International Conference on Advanced Intelligent Mechatronics*, 410–415 (1999).
34. J. S. Mehling, M. A. Diftler, M. Chu, M. Valvo, A minimally invasive tendril robot for in-space inspection. *IEEE/RAS-EMBS International Conference on Biomedical Robotics and Biomechatronics* **1–3**, 423–428 (2006).
35. A. Sadeghi, A. Tonazzini, L. Popova, B. Mazzolai, Robotic mechanism for soil penetration inspired by plant root. *IEEE International Conference on Robotics and Automation*, 3457-3462 (2013).
36. Materials and methods are available as supplementary materials on *Science* Online.
37. A. P. Summers, J. H. Long, Skin and bones, sinew and gristle: The mechanical behavior of fish skeletal tissues. *Fish Physiol.* **23**, 141 (2006).
38. M. Tesch *et al*., Parameterized and scripted gaits for modular snake robots. *Adv. Robot.* **23**, 1131–1158 (2009). doi: 10.1163/156855309X452566
39. K. J. Quillin, Kinematic scaling of locomotion by hydrostatic animals: Ontogeny of peristaltic crawling by the earthworm lumbricus terrestris. *J. Exp. Biol.* **202**, 661–674 (1999). pmid: 10021320
40. C. Hwang, Plastic collapse of thin rings. *J. Aeronaut. Sci.* **20**, 819–826 (1953). doi: 10.2514/8.2868
41. J. A. DeRuntz, P. Hodge, Crushing of a tube between rigid plates. *J. Appl. Mech.* **30**, 391–395 (1963). doi: 10.1115/1.3636567
42. D. K. Sinha, N. R. Chitkara, Plastic collapse of square rings. *Int. J. Solids Struct.* **18**, 819–826 (1982). doi: 10.1016/0020-7683(82)90038-5

ACKNOWLEDGMENTS

We thank L. Matsushige (Scripps Institute of Oceanography) for providing the seahorse specimens; E. Cory and R. Sah (University of California, San Diego) and Pieter Vanderniepen, Manu Dierick, and Luc Van Hoorebeke (Centre for X-ray Tomography of the Ghent University) for assistance in microcomputed tomography of the seahorses; C. Cassidy (University of California, San Diego) for assistance in 3D printing; R. Blob and C. Mayerl (Clemson) for assistance in high-speed videography; V. Sherman (University of California, San Diego) for assistance in compression testing the solid rings; and L. Lundgren (Clemson University), C. Neutens (Ghent University), and W. Shih and R. Ochoa (University of California, San Diego) for insightful discussions. This work was partially supported by the Department of Mechanical Engineering, Clemson University; the School of Mechanical, Industrial, and Manufacturing Engineering, Oregon State University; the von Liebig Entrepreneurism Center, University of California, San Diego; the National Science Foundation, Division of Materials Research, Ceramics Program Grant 1006931; the Multi-University Research Initiative through the Air Force Office of Scientific Research, AFOSR-FA9550-15-1-0009; and the Agency for Innovation by Science and Technology (IWT), grant IWT/SB-111249. The University of California, San Diego, holds the following provisional patent: M. Porter, J. McKittrick, M. Meyers, S. Cai, D. Adriaens, T. Praet, M. De Beule, B. Verhegghe, "Seahorse Inspired Devices" (Application Number 62044058). Data reported, detailed materials and methods, as well as additional discussion and figures are included in the supplementary materials.

SUPPLEMENTARY MATERIALS

www.sciencemag.org/content/349/6243/aaa6683/suppl/DC1
Materials and Methods
Figs. S1 to S8
Table S1
References (*43*–*52*)
Movies S1 and S2

13 January 2015; accepted 14 May 2015
10.1126/science.aaa6683

Why the seahorse tail is square

Michael M. Porter *et al.*

Science **349**, (2015);
DOI: 10.1126/science.aaa6683